Origins and implications of the ordering of oxygen vacancies and localized electrons on partially reduced CeO_{2}(111)

Jonathan E. Sutton, Ariana Beste, and Steven H. Overbury

Phys. Rev. B **92**, 144105 — Published 12 October 2015

DOI: 10.1103/PhysRevB.92.144105

Origins and Implications of the Ordering of Oxygen Vacancies and Localized Electrons on Partially Reduced $CeO_2(111)$

Jonathan E. Sutton, Steven H. Overbury
Chemical Sciences Division, Oak Ridge National Laboratory

Ariana Beste
Computer Science and Mathematics Division, Oak Ridge National Laboratory

We use density functional theory to explain the preferred structure of partially reduced $CeO_2(111)$. Low energy ordered structures are formed when the vacancies are isolated (maximized intervacancy separation) and the size of the Ce^{3+} ions is minimized. Both conditions help minimize disruptions to the lattice around the vacancy. The stability of the ordered structures suggests that isolated vacancies are adequate for modeling more complex (e.g., catalytic) systems. O diffusion barriers are predicted to be low enough that O diffusion between vacancies is thermodynamically controlled at room temperature. The O diffusion reaction energies and barriers are decreased when one Ce f electron hops from a nearest neighbor Ce cation to a next nearest neighbor Ce cation, with a barrier that has been estimated to be slightly less than the barrier to O diffusion in the absence of polaron hopping. This indicates that polaron hopping plays a key role in facilitating the overall O diffusion process, and depending on the relative magnitudes of the polaron hopping and O diffusion barriers, polaron hopping may be the kinetically limiting process.

Keywords: CeO2; O vacancies; density functional theory

I. INTRODUCTION

Ceria is a reducible oxide frequently used as a catalyst[1] and as an electrolyte for solid oxide fuel cells[2] due to its ability to form O vacancies. As a catalyst, it has multiple active sites, including Ce ions and O vacancies.[3] As an electrolyte, charge transport occurs via polaron hopping and O diffusion[4], the latter process being facilitated by O vacancies. Improved understanding of the structure and charge transport kinetics of partially reduced ceria could result in improved ceria-based catalysts and electrolytes.

Partially reduced ceria has been well-studied theoretically and experimentally. To our knowledge, the most extensive calculations for the $CeO_2(111)$ surface to date have been carried out by Li et al.[5] for single vacancies and by Murgida and Ganduglia-Pirovano[6] for double vacancies. When a vacancy is formed by removal of a neutral O atom (hereafter referred to as a neutral O vacancy), two Ce^{4+} ions are reduced to form Ce^{3+} ions, with the additional electrons localized in partially occupied Ce f-orbitals.[7] A seminal experimental study[8] proposed that O vacancies cluster together. Notwithstanding one theoretical study supporting this[9], other experimental[10–12] and theoretical[6,13,14] works suggest that lattice relaxation effects cause vacancies to repel each other, with the prior experimental evidence for vacancy clustering being attributed to fluorine contamination of the ceria crystal[12]. Connected with the formation of O vacancies is the localization of the extra electrons. The current theoretical consensus[5,6,14–18] is that Ce^{3+} ions are located at second neighbor positions to the vacancies. It has been observed that this maximizes the average Ce–O bond length.[5,16] A combination of experimental titration of the localized f electrons with Au atoms and density functional theory calculations also demonstrate that the Ce^{3+} ions prefer the second neighbor positions.[19] Finally, computations[20] showed that the location of Ce^{3+} ions influences O diffusion barriers in partially reduced $CeO_2(111)$.

Several authors have hinted at why (1) vacancies repel and (2) Ce^{3+} ions prefer the next-nearest neighbor position, but we are not aware of any conclusive explanation for these behaviors. Furthermore, the lack of a global geometry search for the lowest energy configuration impedes general conclusions about the underlying processes because it is not known whether currently-accepted minimum energy structures are, in fact, the most stable structures possible. Employing density functional theory (DFT) and carrying out a global search of potential geometries within a 3x3 supercell, we explain the physical origins of both these phenomena in terms of simple lattice properties (coordination numbers, interatomic distances, ionic size, etc.). Finally, we explore the effect of ceria structure on O diffusion.

II. METHODS

DFT calculations for $CeO_2(111)$ were carried out using VASP[21] with PAW pseudopotentials[22,23], and the PBE[24] functional coupled with semi-empirical van der Waals corrections[25] and on-site Coulombic interactions[26] on the Ce f electrons with U = 5 eV, consistent with prior work.[5] As with prior work[5,14,16,17], we restrict ourselves to ferromagnetic states for the Ce^{3+} f electrons. Single and double vacancy calculations were performed using 3x3 supercells, and a few double vacancy calculations using 4x4 supercells were carried out to test the impact of vacancy density on vacancy formation energies (herein all vacancy formation energies are normalized by

the number of vacancies). All slabs contained three O–Ce–O trilayers (bottom trilayer frozen) and 15 Å of vacuum. The 3x3 supercells employed a 2x2x1 Monkhorst-Pack k-point mesh[27], while the 4x4 supercells employed the gamma point alone. Constrained magnetic moments were used to generate pre-converged structures with the desired electronic configuration. Subsequent removal of the constraints yielded the fully optimized structures. O diffusion barriers were determined using climbing image nudged elastic band (NEB) calculations[28,29] with five images linearly interpolated between the initial and final states.

Given the large total number of configurations in a 3x3 supercell for both single and double vacancies (due to combinatorial complexity), and the inherently local nature of DFT geometry optimizations, it can be difficult to locate the global minimum structure. In an attempt to locate the global minimum in the 3x3 supercell, we performed geometry optimizations for a wide range of configurations. We enumerated all possible configurations and retained a single example from each of the symmetry-equivalent sets to generate a minimal set of unique configurations. From prior work[6], we developed heuristics for ranking the stability of each configuration. Then we selected a subset of the possible configurations, taking care to include configurations along the entire energy coninuum. Our heuristics and the set of sampled configurations were updated and refined during the geometry search. We performed a few additional calculations in 4x4 supercells primarily to test the convergence of our 3x3 supercell calculations with respect to supercell size. We tested the ground state two vacancy structure from Ref.[14] as this was similar to our lowest energy configuration for a single vacancy in the 3x3 supercell. We also tested a few additional structures designed to mimic the low energy configurations of two vacancies in a 3x3 supercell in the larger 4x4 supercell. For isolated vacancies, we tested vacancies in up to the third O layer and localized f electrons in up to the second Ce layer. We restricted paired vacancies to the first two O layers and localized f electrons to the first Ce layer. We sampled 48 single vacancy structures (out of 110) and 83 paired vacancy structures (out of 399) for the 3x3 supercells and 8 structures for the 4x4 supercells. Although many structures have very similar energies, we believe the trends are qualitatively correct owing to beneficial error cancellation.

III. RESULTS

A. Lowest Energy Configurations

Four low energy configurations for single and double vacancy structures are depicted in Fig. 1. Our single vacancy structures (Fig. 1, a and b) are structurally and energetically in excellent agreement with the literature as a whole[15–17], and are in near-quantitative agreement with calculations performed by Li et al.[5]. The lowest energy single vacancy configuration (Fig. 1a) has the two Ce^{3+} ions at second neighbors to a subsurface O vacancy. When one of the Ce^{3+} ions moves next to the subsurface O vacancy (Fig. 1b), the vacancy formation energy increases by 0.07 eV due to a compressed bond between the first neighbor Ce^{3+} and the second neighbor surface O along the line of the $Ce^{3+}-O-V-Ce^{3+}$ chain. In the two lowest energy cases, at least one Ce^{3+} ion is second neighbor to the vacancy, consistent with prior STM and DFT results[17]. The double vacancy structures (Fig. 1, c and d) show similar behavior. In the lowest energy two vacancy structure in a 3x3 supercell (Fig. 1c), each vacancy has both a first neighbor and a second neighbor Ce^{3+} ion. The first vacancy prefers the subsurface, with the second vacancy showing no clear preference for the surface or subsurface (the energy difference is less than 0.02 eV). Decreasing the vacancy concentration by moving to the 4x4 supercell (Fig. 1d) permits all Ce^{3+} ions are to be second neighbors to subsurface O vacancies and to each other. In the 4x4 supercell, vacancies are situated such that both vacancies are in the subsurface, and the distance between vacancies is maximized.

All low energy configurations have the Ce^{3+} ions located at no further than the second neighbor position. This second neighbor ordering (Fig. 1, a and d) and, to a lesser extent, the mixed first and second neighbor ordering (Fig. 1, b and c) results in the construction of periodic domains of $Ce^{3+}-O-V$ chains. Such chains permit a more efficient relaxation of the lattice than that achievable when Ce^{3+} ions are located either further away from or closer to the vacancy. Similar ordered structures have been observed experimentally via AFM by Torbrügge et al.[10] and via STM by Grinter et al.[31]. Torbrügge et al. suggested that the structure of defective ceria is driven by an interplay of short-range interactions.

B. Trends in Vacancy and Ce^{3+} Ion Locations

To better elucidate the exact nature of the short-range interactions driving the surface geometry, we examine trends in the vacancy energies for a number of elementary descriptors as a function of the number of vacancies (one or two) and supercell size (3x3 or 4x4) for two vacancies. Vacancy formation energies are generally similar for both single and double vacancies.

Single vacancies preferentially form in the second O layer (Fig. 2a) compared to the first[5,16,32,33] and third[32,33] O layers, with third layer sites being strongly disfavored. This preference is explained in Fig. 2b by the average coordination number of Ce ions neighboring the vacancy (we assume Ce–O coordination only if the center-to-center distance is less than 2.6 Å, compared to a normal distance of 2.4 Å in the unrelaxed lattice). We use this quantity as a surrogate for the amount and type of lattice reconstruction involved.

In all cases first neighbor O ions move towards the va-

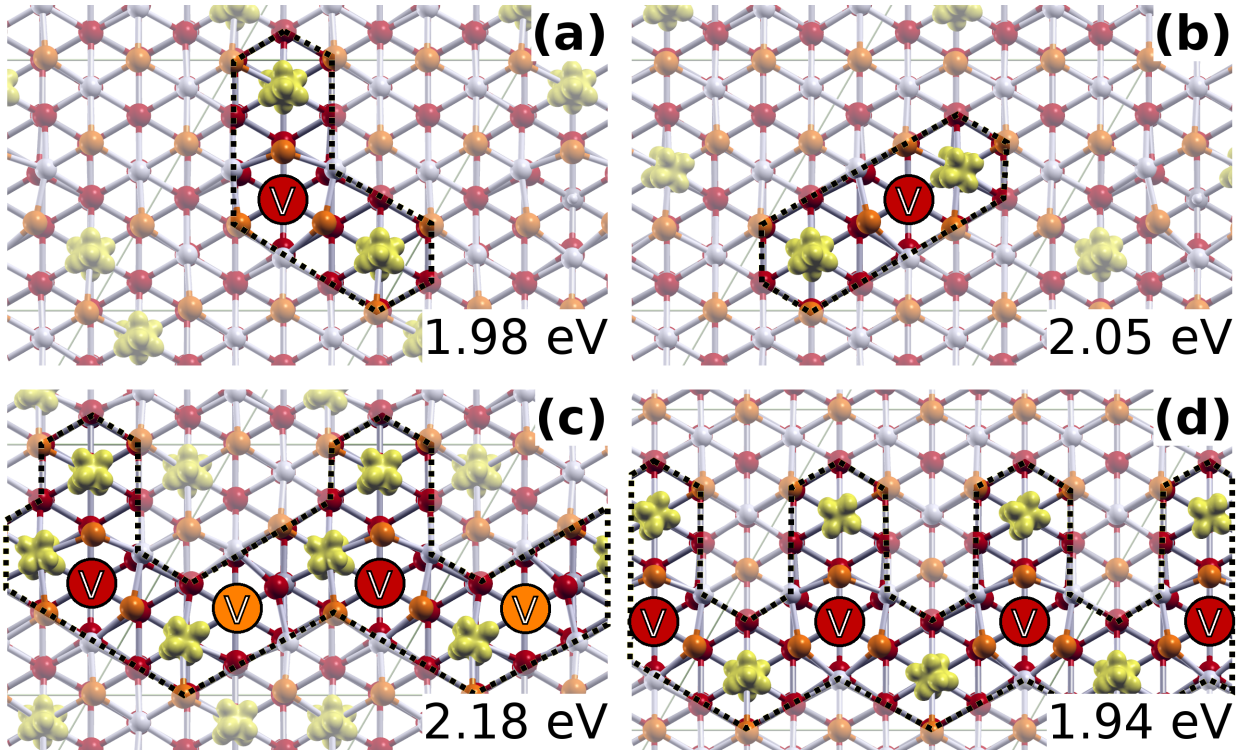

FIG. 1. (Color online.) Selected low energy relaxed structures with one (a, b) and two (c, d) vacancies. Panels (a–c) are for 3x3 supercells, and panel (d) is for a 4x4 supercell. Formation energies per vacancy (eV) are given in the lower right of each panel. Ce^{4+}, surface O, and subsurface O ions are represented by light gray (or off-white), orange, and red spheres. The letter V in a circle denotes a vacancy, with orange (red) circles corresponding to vacancies in the first (second) O layer. Ce^{3+} ions are represented by yellow spin density isosurfaces. Sphere sizes for the Ce^{3+} and O atoms are based on their crystal radii[30]. All low energy structures form at least one Ce^{3+}−O−V chain, with the lowest energy structures (e.g., a and d) forming multiple chains. These chains are highlighted by the dashed lines.

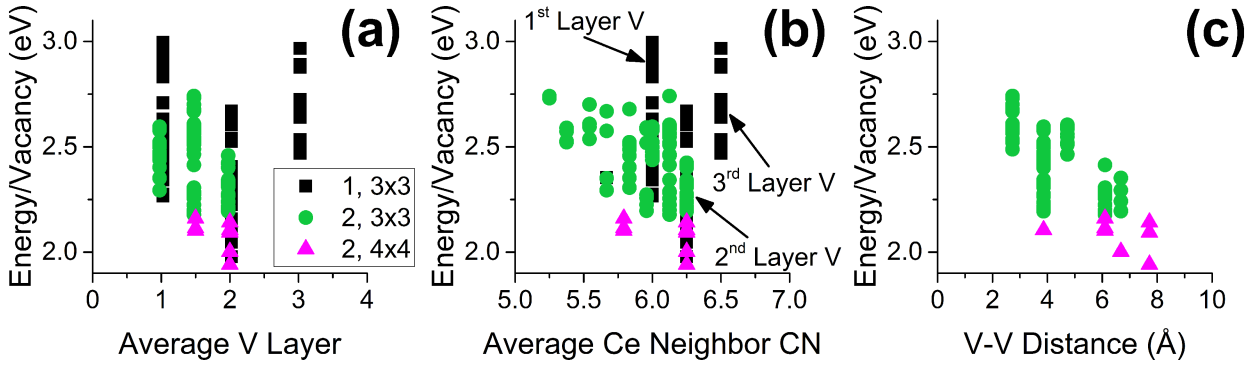

FIG. 2. (Color online.) Plots of trends in the vacancy formation energy for (a) the average O layer in which a vacancy (V) is located, (b) the average coordination number (CN) of the Ce ions that are first neighbors to vacancies, and (c) the intervacancy separation distance. The intervacancy separation for a single vacancy in a 3x3 supercell is 12 Å. Data points for single (double) vacancies in 3x3 supercells are in black (green). Data points for double vacancies in 4x4 supercells are in magenta.

cancy and displace or reduce the coordination number of neighboring Ce ions. A third layer vacancy pushes the neighboring surface Ce ion upward, out of its plane, by 0.35 Å, decreasing the coordination number of it and its six second neighbor surface Ce ions. First layer vacancies induce a more moderate amount of lattice reconstruction, reducing the coordination numbers of three first neighbor surface Ce ions and three second neighbor subsurface Ce ions. Second layer vacancies result in only minor lattice reconstruction with no more than three surface Ce ions having reduced coordination numbers. Further, placing the two Ce^{3+} ions in second neighbor positions to the subsurface vacancy (e.g. as in Fig. 1a) beneficially reduces their coordination number and ionic size (Table S1,

Supplementary Material[34]), with a corresponding energy decrease.

Double vacancies exist preferentially when both are in the second layer (4x4 supercell) or when one is in each of the first and second layers (3x3 supercell), giving an average O layer of 1.5 (Fig. 2a). The preference for the mixed first and second O layer configuration in 3x3 supercells is due to the preference for the second O layer being offset by the penalty arising from having to put two defects in close proximity to each other (via the periodic boundary). This penalty does not arise in the 4x4 supercell, and there is about a 0.25 eV decrease in the vacancy formation energy.

In the case of double vacancies, vacancy formation energies are minimized (Fig. 2b) when the average coordination number of neighboring Ce ions is around 6.25 (the same as for the single vacancy case). Vacancy formation energies in 4x4 supercells are similar to the vacancy formation energies for a single vacancy in 3x3 supercells. Preferred vacancy locations (O layer and average Ce coordination number) are also similar, which is not surprising given the similar vacancy concentrations in the top three oxygen layers for 3x3 and 4x4 supercells (1/27 and 2/48, respectively). However, in the case of two vacancies in 3x3 supercells (vacancy concentration of 2/27), the average Ce neighbor coordination number no longer clearly indicates the preferred O layers. Instead, the energy depends more strongly on the vacancy separation distance, with low energy structures requiring at least second neighbor separation (around 4 Å, Fig. 2c). Average vacancy separations of around 5 Å result in the formation of high energy linear V–Ce–V structures (more details are in the Supplementary Material[34]). Fourth and fifth neighbors in 3x3 supercells are marginally lower in energy than vacancies located at second neighbors to each other. Increasing the supercell size permits increased separation distances between two in-cell vacancies (maximum of around 8 Å) and a further decrease in the vacancy formation energy. Increasing the separation distance to 12 Å (single vacancy separation via periodic boundary conditions in a 3x3 supercell) yields an average vacancy formation energy nearly identical to the average energy of two vacancies separated by 8 Å. The preference for vacancies to maximize their separation suggests that single vacancy supercells may be adequate for modeling catalytic and electrochemical processes on moderately reduced surfaces.

As previously noted, the locations of the Ce^{3+} ions play a key role in the vacancy formation energy. Upon reduction, Ce ions grow in size, and this in turn, impacts the favorable locations for the Ce^{3+} ions. In tests with single vacancies (Fig. 3a), we find that Ce^{3+} ions strongly prefer the first Ce layer. The preference of Ce^{3+} ions for the surface correlates extremely well with the average Ce^{3+} coordination number (Fig. 3b), with lower energies being associated with smaller coordination numbers (and hence smaller ionic radii[30], Table S1[34]). The smaller ionic radius associated with the surface cations

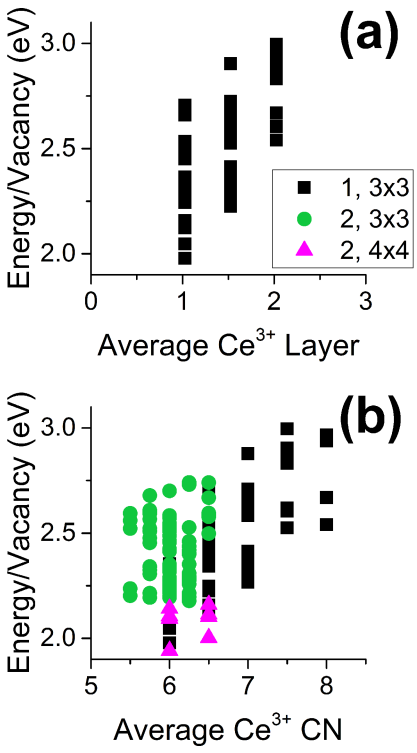

FIG. 3. (Color online.) Plots of trends in the vacancy formation energy for (a) the average Ce layer in which the Ce^{3+} ions are located and (b) the average coordination number of the Ce^{3+} ions. Data points for single (double) vacancies in 3x3 supercells are in black (green). Data points for double vacancies in 4x4 supercells are in magenta.

makes it easier for them to fit into the surrounding lattice. We expect that a similar trend applies to double vacancies as well, so we restricted our double vacancy calculations to configurations where the Ce^{3+} ions were in the surface layer.

Ce coordination numbers and oxidation states are responsible for Ce^{3+} ions preferentially occupying second neighbor positions to the vacancy. Part of this preference is that the second neighbor Ce positions are 6-coordinated, with an accompanying decrease in size of the occupying Ce ion. The coordination number alone, however, is insufficient to explain the preference as the first neighbor Ce sites have the same coordination number (six) as the second neighbor Ce sites. The second factor is that when the first neighbor O ions move towards the vacancy, they simultaneously push the first neighbor Ce ions away from the vacancy, compressing a Ce–O bond in the process. This displacement and bond compression is more easily accepted by the smaller 6-coordinated Ce^{4+} ions (1.0 Å radius) than by the larger 6-coordinated Ce^{3+} ions (1.15 Å radius). This 0.25 eV compression is avoided by placing the Ce^{3+} ions in the more spacious second neighbor positions.

Interestingly, some of these effects are also observed in doped ceria materials. The size and oxidation state of the cation dopant can affect both the vacancy for-

mation energy as well as the preferred location of the dopant. Smaller non-reducible isovalent ions (e.g., Zr^{4+}) or aliovalent ions (e.g., La^{3+}) lower the vacancy formation energy via primarily geometric and electronic means, respectively.[35] Cation radius has also been found to control the preferred location of the dopant relative to the vacancy. Dopants with radii larger than that of Gd (e.g., Ce^{3+}) prefer the second neighbor position, and those with smaller radii prefer the first neighbor position.[36]

C. O Diffusion Pathways

Finally, Ce oxidation states and vacancy concentration together influence the barrier to O diffusion within the lattice. We consider four possible diffusion pathways, as depicted in Fig. 4. Each of the pathways involves at least one of the stable structures in Fig. 1. In an attempt to decouple O diffusion and electron transfer via polaron hopping, all pathways involve the diffusion of a subsurface vacancy to the surface in the presence of fixed Ce^{3+} ion locations. In the first path (Fig. 4a), the Ce^{3+} ions are second neighbors to the initial subsurface vacancy. In the second path (Fig. 4b), the initial vacancy has one second neighbor Ce^{3+} ion and one first neighbor Ce^{3+} ion. The third path (Fig. 4c), is similar to the second, except that a second subsurface vacancy is present in the supercell. Finally, the fourth path is similar to the third path, but the supercell is larger, and the Ce^{3+} ions for the second vacancy are placed at the more favorable second neighbor positions.

The energy profiles for the four pathways are presented in Fig. 5. Vibrational frequency calculations at the highest energy points along the paths yield only real frequencies and unconstrained geometry optimizations result in only minor geometry relaxation, showing that they are stationary points or intermediates rather than transition states. The potential energy surfaces are rather flat (the minimum vibrational frequency calculations are all smaller than 100 cm^{-1}), making it difficult to locate the actual transition states. Nevertheless, we believe these stationary states are likely close to the transition states both geometrically and energetically, and we approximate the activation energy as the difference between the high energy stationary state and the energy of the initial state.

In all cases, the highest energy along the path Fig. (5a) is very similar to the final state energy, a fact highlighted by the high degree of correlation between the approximate activation energy and the reaction energy (Fig. 5b). The highest energy locations along the path are when the O anions are located in the interstices between two Ce cations, a finding we believe to be independent of the Ce^{3+} cation locations. In the absence of electron transfer via polaron hopping, the approximate activation energy is nearly identical to the reaction energy, and O diffusion in partially reduced ceria will be controlled by thermodynamics.

The thermodynamic control of O diffusion in the absence of polaron hopping leads to an interesting possibility regarding the kinetics of vacancy equilibration. In path (a), the O diffusion is endothermic by 0.53 eV because one of the Ce^{3+} ions in the final state is 7-coordinated (as outlined earlier, this CN results in a Ce^{3+} ion that is too large for the surrounding lattice). Placing an f electron next to the vacancy (Fig. 4b) results in a slightly less stable initial state (by 0.07 eV) but a much more stable final state (0.23 eV reaction energy) because both Ce^{3+} ions always remain 6-coordinated, and the Ce^{3+} ion radii do not change during the O diffusion process (a similar effect also occurs with paths (c) and (d) where two vacancies are present). It has been estimated with DFT that the barrier to convert the initial structure in Fig. 4a to the initial structure in Fig. 4b via polaron hopping is just 0.29 eV, and other distributions of Ce^{3+} ions all have barriers to polaron hopping lower than 0.5 eV.[20] Experimentally determined polaron hopping barriers are also below about 0.5 eV.[37,38] Significantly, polaron hopping is activated with low barriers similar to or larger than the reaction energy associated with O diffusion in the less endothermic path (b). This leads to an interesting conclusion; the kinetics of the O diffusion process may be controlled by the barrier to polarons hopping between Ce cations.

Increasing the concentration of vacancies increases the stability of the final states (i.e., where one O vacancy is at the surface), with an accompanying decrease in the approximated O diffusion barriers. In other words, adding a vacancy improves the stability of O anions in intersitial sites. The additional vacancy produces a lattice with more flexibility and with O anions that are closer to the interstitial sites. This effect is minimal for two vacancies in a 4x4 supercell (vacancy concentration of 2/48, Fig. 5b, point d), but it is quite pronounced for two vacancies in a 3x3 supercell (vacancy concentration of 2/27, Fig. 5b, point c). In the last case, the diffusion is nearly thermoneutral with an approximated barrier of only 0.05 eV. With such low barriers, especially at moderate vacancy concentrations, it becomes even more likely that the distribution of O vacancies is controlled by the kinetics of polaron hopping, a process with a fairly low barrier. At room temperature or above, polaron hopping will be fast and equilibrated. As a result, O vacancy exchange between the surface and subsurface is likely to be rapid and thermodynamically-controlled on the $CeO_2(111)$ surface.

IV. CONCLUSIONS

Low energy ordered structures form due to interplay between intervacancy separation distance and Ce^{3+} ionic radius. Neutral O vacancies concentrate in the subsurface with maximal intervacancy separation as this results in the least disruption to the surrounding lattice. Maximized intervacancy separation implies supercells with isolated vacancies can be adequate for modeling catalytic

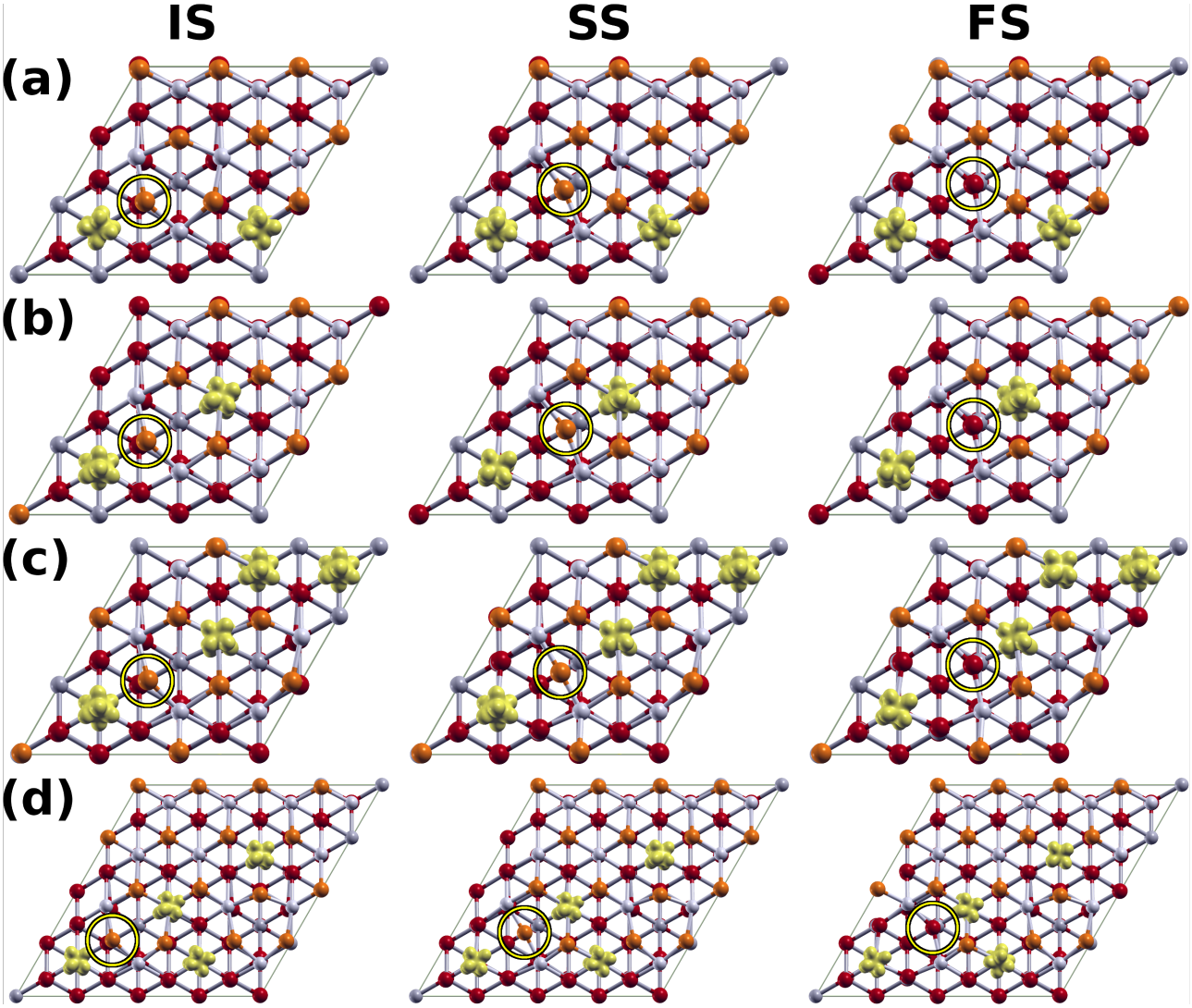

FIG. 4. Initial state (IS), high energy stationary state (SS), and final state (FS) images of the O diffusion pathways in the presence of one (a and b) and two (c and d) vacancies. Panels a–c are in 3x3 supercells, and panel d is in a 4x4 supercell. Panel labels correspond to the labeled pathways in Fig. 5a. The diffusing O is highlighted by the black-outlined circle in each image.

surfaces. The additional electrons left by the neutral O localize on Ce ions that are second neighbors to the vacancies to take advantage of the decreased ionic size and additional space that results from the first neighbor O ions moving towards the vacancy. We find that O diffuses from the surface to the subsurface by passing through interstitial sites with energies that are nearly identical to the energy of the final states. The reaction thermodynamics are directly related to the positions of the f electrons relative to the vacancy. When both Ce^{3+} ions always have a coordination number of six, the reaction energy is minimized. The interstitial O energy is reduced by the presence of a second O vacancy in the lattice. The estimated O diffusion barriers are similar to or smaller than estimated barriers for polaron hopping, suggesting that electron transport may control both the thermodynamics and kinetics of O anion diffusion through the lattice.

V. ACKNOWLEDGMENTS

This research was sponsored by the Laboratory Directed Research and Development Program of Oak Ridge National Laboratory, managed by UT-Battelle, LLC, for the U.S. Department of Energy. This research used resources of the Oak Ridge Leadership Computing Facility at the Oak Ridge National Laboratory, which is supported by the Office of Science of the U.S. Department of Energy under Contract No. DE-AC05-00OR22725.

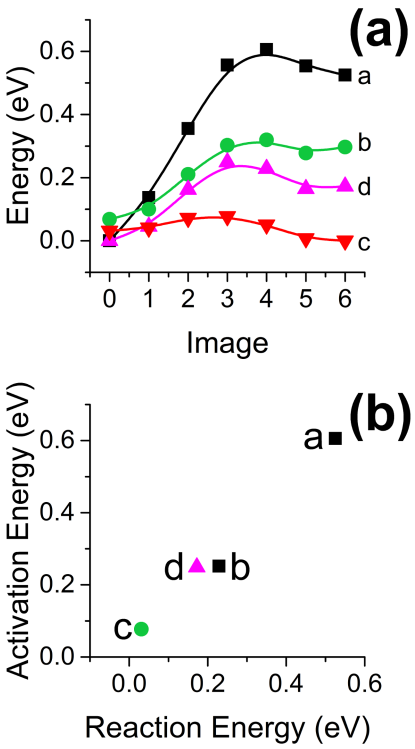

FIG. 5. (a) Energy profiles (relative to lowest energy configuration for a given supercell size) of O diffusion from the surface to the subsurface corresponding to the structures in Fig. 4. (b) Summary of approximate activation and reaction energies for the O diffusion pathways.

[1] A. Trovarelli, Catalysis Reviews **38**, 439 (1996), vl751 Times Cited:1741 Cited References Count:333.

[2] S. Park, J. M. Vohs, and R. J. Gorte, Nature **404**, 265 (2000).

[3] D. R. Mullins, Surface Science Reports **70**, 42 (2015).

[4] J. J. Plata, A. M. Márquez, and J. F. Sanz, Journal of Physical Chemistry C **117**, 14502 (2013), 187VR Times Cited:4 Cited References Count:55.

[5] H.-Y. Li, H.-F. Wang, X.-Q. Gong, Y.-L. Guo, Y. Guo, G. Lu, and P. Hu, Physical Review B **79** (2009), 10.1103/PhysRevB.79.193401.

[6] G. E. Murgida, V. Ferrari, M. V. Ganduglia-Pirovano, and A. M. Llois, Physical Review B **90** (2014), 10.1103/PhysRevB.90.115120.

[7] N. V. Skorodumova, S. I. Simak, B. I. Lundqvist, I. A. Abrikosov, and B. Johansson, Physical Review Letters **89** (2002), 10.1103/PhysRevLett.89.166601, times Cited: 288 Skorodumova, NV Simak, SI Lundqvist, BI Abrikosov, IA Johansson, B Lundqvist, Bengt/A-9013-2011; Simak, Sergei/C-3030-2014 Simak, Sergei/0000-0002-1320-389X 295 1079-7114.

[8] F. Esch, S. Fabris, L. Zhou, T. Montini, C. Africh, P. Fornasiero, G. Comelli, and R. Rosei, Science **309**, 752 (2005), times Cited: 455 Esch, Friedrich/A-3678-2010; Fornasiero, Paolo/B-7279-2011; Montini, Tiziano/G-3363-2011; Fabris, Stefano/B-6907-2008 Esch, Friedrich/0000-0001-7793-3341; Fornasiero, Paolo/0000-0003-1082-9157; Fabris, Stefano/0000-0003-2562-8788 0 468.

[9] C. Zhang, A. Michaelides, D. A. King, and S. J. Jenkins, Physical Review B **79** (2009), 10.1103/PhysRevB.79.075433, times Cited: 47 Michaelides, Angelos/K-8727-2012 0 48.

[10] S. Torbruegge, M. Reichling, A. Ishiyama, S. Morita, and O. Custance, Physical Review Letters **99** (2007), 10.1103/PhysRevLett.99.056101, times Cited: 68 Reichling, Michael/B-1123-2011 0 68.

[11] D. C. Grinter, R. Ithnin, C. L. Pang, and G. Thornton, Journal of Physical Chemistry C **114**, 17036 (2010), times Cited: 34 ithnin, roslinda/B-9613-2010 0 34.

[12] J. Kullgren, M. J. Wolf, C. W. M. Castleton, P. Mitev, W. J. Briels, and K. Hermansson, Physical Review Letters **112** (2014), 10.1103/PhysRevLett.112.156102, times Cited: 2 0 2.

[13] J. L. Ma, F. Ye, D. R. Ou, L. L. Li, and T. Mori, Journal of Physical Chemistry C **116**, 25777 (2012), times Cited: 1 0 1.

[14] G. E. Murgida and M. V. Ganduglia-Pirovano, Physical Review Letters **110** (2013), 10.1103/PhysRevLett.110.246101.

[15] J. C. Conesa, Catalysis Today **143**, 315 (2009), times Cited: 28 Conesa, Jose/H-6277-2011 Conesa, Jose/0000-0001-9906-8520 0 29.

[16] M. V. Ganduglia-Pirovano, J. L. F. Da Silva, and J. Sauer, Physical Review Letters **102** (2009), 10.1103/PhysRevLett.102.026101.

[17] J.-F. Jerratsch, X. Shao, N. Nilius, H.-J. Freund, C. Popa, M. V. Ganduglia-Pirovano, A. M. Burow, and J. Sauer, Physical Review Letters **106**, 246801 (2011), jerratsch, Jan-Frederik Shao, Xiang Nilius, Niklas Freund, Hans-Joachim Popa, Cristina Ganduglia-Pirovano, M Veronica Burow, Asbjorn M Sauer, Joachim eng 2011/07/21 06:00 Phys Rev Lett. 2011 Jun 17;106(24):246801. Epub 2011 Jun 14.

[18] E. Shoko, M. F. Smith, and R. H. McKenzie, Journal of Physics: Condensed Matter **22**, 223201 (2010), shoko, E Smith, M F McKenzie, Ross H eng England 2011/03/12 06:00 J Phys Condens Matter. 2010 Jun 9;22(22):223201. doi: 10.1088/0953-8984/22/22/223201. Epub 2010 May 21.

[19] Y. Pan, N. Nilius, H.-J. Freund, J. Paier, C. Penschke, and J. Sauer, Phys. Rev. Lett. **111**, 206101 (2013).

[20] J. J. Plata, A. M. Márquez, and J. F. Sanz, Journal of Physical Chemistry C **117**, 25497 (2013).

[21] G. Kresse and J. Furthmuller, Physical Review B **54**, 11169 (1996), times Cited: 21624 Furthmueller, Juergen/B-2346-2008 1 21829.

[22] P. E. Blochl, Physical Review B **50**, 17953 (1994), times Cited: 15101 Blochl, Peter/B-3448-2012 Blochl, Peter/0000-0002-1416-5207 3 15180.

[23] G. Kresse and D. Joubert, Physical Review B **59**, 1758 (1999), times Cited: 15951 1 16074.

[24] J. P. Perdew, K. Burke, and M. Ernzerhof, Physical Review Letters **77**, 3865 (1996).

[25] S. Grimme, J. Antony, S. Ehrlich, and H. Krieg, The Journal of Chemical Physics **132**, 154104 (2010).

[26] S. L. Dudarev, G. A. Botton, S. Y. Savrasov, C. J. Humphreys, and A. P. Sutton, Physical Review B **57**, 1505 (1998), times Cited: 2304 0 2317.

[27] H. J. Monkhorst and J. D. Pack, Physical Review B **13**, 5188 (1976), times Cited: 18883 10 19204.

[28] G. Henkelman and H. Jónsson, The Journal of Chemical Physics **113**, 9978 (2000).

[29] G. Henkelman, B. P. Uberuaga, and H. Jnsson, The Journal of Chemical Physics **113**, 9901 (2000).

[30] R. Shannon, Acta Crystallographica Section A **32**, 751 (1976).

[31] D. C. Grinter, C. L. Pang, C. A. Muryn, F. Maccherozzi, S. S. Dhesi, and G. Thornton, Journal of Electron Spectroscopy and Related Phenomena **195**, 13 (2014), times Cited: 1 0 1.

[32] S. Shi, Y. Tang, C. Ouyang, L. Cui, X. Xin, P. Li, W. Zhou, H. Zhang, M. Lei, and L. Chen, Journal of Physics and Chemistry of Solids **71**, 788 (2010), times Cited: 11 Shi, Siqi/E-1245-2011 0 13.

[33] V. Botu, R. Ramprasad, and A. B. Mhadeshwar, Surface Science **619**, 49 (2014).

[34] See Supplemental Material at [URL] for additional information on the crystal radii and images of converged structures.

[35] J. Paier, C. Penschke, and J. Sauer, Chemical Reviews **113**, 3949 (2013), paier, Joachim Penschke, Christopher Sauer, Joachim eng 2013/05/09 06:00 Chem Rev. 2013 Jun 12;113(6):3949-85. doi: 10.1021/cr3004949. Epub 2013 May 7.

[36] E. Shoko, M. F. Smith, and R. H. McKenzie, Journal of Physics and Chemistry of Solids **72**, 1482 (2011), times Cited: 10 McKenzie, Ross/D-8900-2013 0 10.

[37] H. L. Tuller and A. S. Nowick, Journal of Physics and Chemistry of Solids **38**, 859 (1977), dr860 Times Cited:375 Cited References Count:31.

[38] I. K. Naik and T. Y. Tien, Journal of Physics and Chemistry of Solids **39**, 311 (1978), times Cited: 117 0 117.